Eur. Phys. J. B **31**, 273–284 (2003)
DOI: 10.1140/epjb/e2003-00032-8

THE EUROPEAN PHYSICAL JOURNAL B

Some novel three-dimensional Euclidean crystalline networks derived from two-dimensional hyperbolic tilings

S.T. Hyde[a] and S. Ramsden

Applied Mathematics Department, Research School of Physical Sciences, Australian National University, Canberra, 0200 A.C.T., Australia

Received 14 January 2002 / Received in final form 12 August 2002
Published online 4 February 2003 –

Abstract. We demonstrate the usefulness of two-dimensional hyperbolic geometry as a tool to generate three-dimensional Euclidean (E^3) networks. The technique involves projection of edges of tilings of the hyperbolic plane (H^2) onto three-periodic minimal surfaces, embedded in E^3. Given the extraordinary wealth of symmetries commensurate with H^2, we can generate networks in E^3 that are difficult to construct otherwise. In particular, we form four-, five- and seven-connected (E^3) nets containing three- and five-rings, *viz.* (3, 7), (5, 4) and (5, 5) tilings in H^2.

PACS. 89.75.Kd Patterns – 89.75.Hc Networks and genealogical trees – 82.75.Fq Synthesis, structure determination, structure modeling

Introduction

The motivation for this work lies in our poor knowledge of networks in three-dimensional Euclidean space (E^3). The nature of E^3 presents obstacles to net formation that are not yet well understood. Those obstacles are in part *geometric*. Thus, for example, a locally preferred packing configuration corresponding to tetrahedrally close-packed arrangements of vertices is unrealizable in E^3, but accessible in 3D elliptic space. In a series of papers, Sadoc, Mosseri and Rivier have argued that many atomic configurations in glasses and alloys (particularly Frank-Kasper phases and their duals) are frustrated attempts to decurve those elliptic configurations, involving networks of disclinations, and thereby mapping the elliptic geometries back to E^3 (Ref. [1]). A number of conjectures concerning accessible ring-sizes in four-connected nets have been made by chemists that remain intriguing yet unproven [2]. It is possible that there are, in addition, *topological* obstacles to net formation in E^3, where certain network topologies are unrealizable with *any* geometry in flat 3D space. To cite just one example, we know of no example of four-connected networks whose smallest rings are all pentagons [3]. Despite the corpus of data on networks gathered by solid state chemists, it is fair to state that we remain in a state of profound ignorance of the variety of nets realizable in E^3. Substantial progress in experimental determination of structures to high resolution of atomic and molecular crystals has not been mirrored by corresponding progress in fundamental understanding of *possible* structures in E^3. We have not advanced much beyond empirical construction of nets, despite the importance of networks in areas as diverse as crystal engineering [4] and small-worlds theory [5]. An important exception is the recent advance in systematic enumeration of a restricted class of four-connected nets in E^3 (Ref. [6]).

It has long been recognized that crystalline networks, particularly those of low vertex density (normalized to nets of unit edge length) are decorations of triply periodic minimal surfaces, or topologically identical surfaces [7,8]. Here we formalize somewhat that construction, and focus on examples that are intractable within the confines of conventional Euclidean crystallography. Net(work)s are constructed with pentagonal rings and containing equivalent seven-connected vertices.

This paper offers some examples of a novel technique to construct nets *ab initio*. The technique is almost exclusively confined to 2D geometry, where the third dimension of E^3 is subsumed within a parameter available to non-Euclidean geometries, curvature. Rather than working within flat 3D space (E^3), we construct the unwrapped net in 2D hyperbolic space, H^2 and then project H^2 onto E^3, *via* triply periodic minimal surfaces.

Construction of 3D Euclidean nets from the hyperbolic plane

The approach involves the formation of a net in its universal cover. There is a simple analogy to cylindrical nets, well developed to characterise carbon tubule structures. In

[a] e-mail: stephen.hyde@anu.edu.au

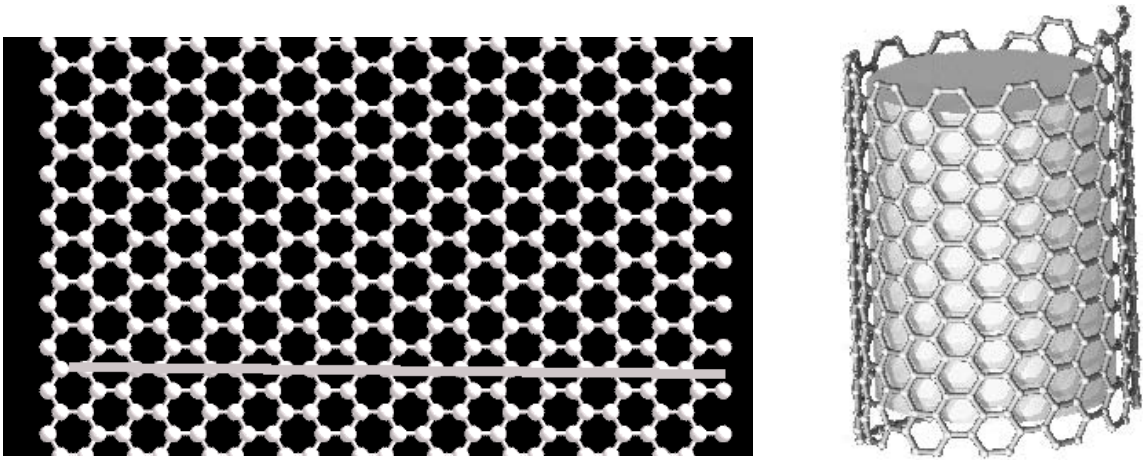

Fig. 1. Mapping $\{6, 3\}$ to carbon tubule nets: (a) the graphite network is rolled gluing ends of the (grey) equatorial line, forming the tubular network in (b). The length and orientation of that line determines the tubule radius and chirality resp. (Tubule image courtesy of D. Tomanek.)

that case, the sp^2 graphite net tiles a cylinder. The (surface averaged) Gaussian curvature of a cylinder (or any extended rod-shaped surface) is zero, and the cylinder is Euclidean. Its universal cover is the Euclidean plane (E^2). The graphite net can be realized as a regular tiling of E^2, with identical vertices, all belonging to three hexagonal rings; we denote the net by a modified Schläfli symbol, (6, 3). (The regular form of (6, 3), with symmetrically identical hexagonal faces, edges and vertices, is denoted $\{6, 3\}$.) Tubule nets can be generated by projecting the (6, 3) net onto a cylinder, formed by gluing net components separated by a fixed gluing vector traced on E^2. The infinite (6, 3) pattern in the unbounded Euclidean plane, E^2, is thus an infinite-sheeted cover of the cylindrical tiling. A realisable carbon tubule structure derived from graphite corresponds to the identification of any 1D lattice on the (6, 3) net (Fig. 1). The gluing vector defines an equatorial loop around the cylinder and the cylinder dimensions relative to the edge length of the (6, 3) tiling. Gluing vectors that are coincident with reflection lines of the $\{6, 3\}$ net result in achiral tubule structures. Generic chiral examples, related to the achiral ones by screw dislocations, are generated by gluing vectors that are inclined to all reflection lines of the $\{6, 3\}$ net.

Generalisation of this concept allows us to systematically derive examples of a restricted° — but large — subset of all crystalline nets in E^3. Those nets tile hyperbolic surfaces, and can be embedded without altering their topology (though likely their geometry: edge lengths and vertex positions). The universal cover [9] of hyperbolic surfaces is the hyperbolic plane, H^2, which can be considered as a multiple-copy of the unfolded three-periodic surface, just as the Euclidean plane is the universal cover of the cylinder. We can generate nets on three-periodic surfaces in E^3, that form crystalline nets in E^3, *via* tilings of H^2. The nets contain surface rings, visible in the H^2 tiling and collar rings, that are the result of the projection (or gluing) from H^2 to the surface.

There is a significant extra complication in this construction that is not present in the cylindrical examples. It arises from the requirement that H^2 be distorted in order to project in onto E^3. In practice, the Gaussian curvature of three-periodic hyperbolic surfaces must vary over the surface, in contrast to the fixed (negative) Gaussian curvature of H^2. The isotropic H^2 space is distorted, and a conformal group structure imposed on H^2 to allow projection onto E^3. The conformal structure can be made exact for the case of three-periodic minimal surfaces, as follows. These surfaces are made up of asymmetric surface patches (*Flächenstücke*) bounded by special curves that are intrinsic mirrors in the surface [10]. Those mirrors emanate from the isolated singular points on the minimal surface of zero Gaussian curvature; the flat points. Their type and locations are defined by the Gauss map of the surface, used to explicitly parametrise the surface embedding in E^3. Those curves correspond to special directions on the surface (principal or asymptotic directions, with the exception of the gyroid) and intersect at $\frac{1}{4}/4$ or $\frac{1}{4}/2$ at all points with possible exception of flat points.

We consider here only the simplest three-periodic minimal surfaces, the P and D surfaces (and, in passing, the hexagonal H surface). The Gauss maps of their *Flächenstücke*, resident in the 2D complex plane, C^2 (derived in Ref. [10]) are polygons whose edges are circular arcs. The complete surface is generated by reflection in the edges of the polygon. The Gauss map is a conformally faithful representation of the surface geometry in E^3, except at flat points (i), where it is multiplied by the order b_i of the flat point. These polygons, with suitably rescaled vertex angles at vertices corresponding to flat points, thus offer a convenient conformal map for the three-periodic minimal surface geometry in its universal cover (H^2) [11]. The relevant polygons in C^2 are shown in Figures 2. Note that the P and D surfaces are intrinsically identical — only their E^3 embeddings differ — so that their *Flächenstücke* are indistinguishable.

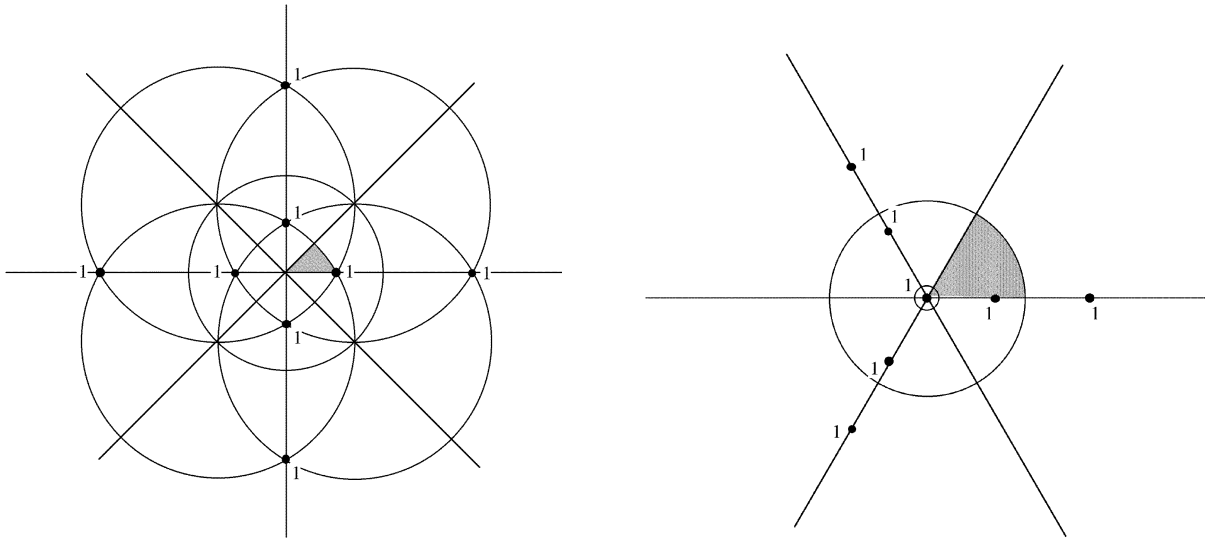

Fig. 2. Complex plane representation of the Gauss map of the P and D three-periodic minimal surfaces (a) and the H surface (b). The maps contain asymmetric tiles (shaded) that generate the complete map by reflection in the tile edges. Flat points on the tile edges are marked by a dot and the numeral 1, denoting that these are first-order flat points. The P/D surface tile contains three vertices, the H surface tile four, counting the flat point along an edge. (The open circle at the origin in (b) denotes an extra first order flat point at 8.)

This construction allows (in principle) an exact conformal map from H^2 to the surface. We are principally concerned with the topological structure of the nets on these surfaces, and their geometry is later relaxed in E^3, so we refrain here from explicit description of that map (that has, in any case, yet to be explicitly determined in most cases).

The conformal maps on H^2 impose a group structure on that space, as the *Flächenstücke* polygons are mirrors. The hyperbolic crystallography of these surfaces is thus a sub-group of the (kaleidoscopic) group defined by these mirrors. The full group defines the relevant group of the universal cover of the surface — unglued into the disc-like hyperbolic plane, and replicated. The three-periodic minimal surface contains relations in addition to the mirrors, defining the gluing pattern needed to (i) stitch the surface up from H^2 (identical to the gluing lines for cylinders from E^2) and (ii) account for the Euclidean translations of the lattice underlying these periodic surfaces. A detailed account of this procedure for the P and D surfaces can be found elsewhere [12]. Those relations must be respected in any tiling superposed on H^2, to ensure the projected tiling, a net in E^3, is commensurate with the surface and contains the same translational symmetries as those of the underlying surface. (We could relax that constraint, and allow supercells of the surface lattice; here we neglect that possibility.) In order to reticulate the three-periodic minimal surface in a commensurate fashion, the starting tiling in H^2 is chosen to be a sub-group of the kaleidoscopic group of the surface's universal cover and a supergroup of the translations in the compactified unit cell of the surface that results from applying gluings of types (i) and (ii) above. This compact surface is a three-handled torus.

The hyperbolic crystallography of these surfaces can be neatly described using the orbifold concept, developed by Conway and Thurston [13]. An orbifold contains a single asymmetric unit of the symmetric 2D pattern, suitably compactified. Conway's notation is particularly useful, as it is generic to the three possible 2D non-Euclidean geometries: elliptic (spherical 2D groups, the crystallographic point groups), parabolic or Euclidean (planar 2D "wallpaper" groups) and hyperbolic. There are only four possible symmetry elements of these 2D groups: mirror lines, glide lines, rotation centers and translations. Each distinct symmetry element that is not derivable from other elements contributes a symbol to the orbifold symbol string. For our purposes, we need to consider only orbifolds containing rotation centers (denoted by the numeral a, where the rotation center defines an a-fold rotational center and mirror lines (contributing a single "*" character per disjoint mirror circuit). Rotation centers lying on intersections of mirror lines subtending angles of $\frac{\pi}{b_1}, \frac{\pi}{b_2}, \ldots$ lead to the "$*b_1\ b_2$" character string. For example, the pattern in the complex plane due to the Gauss map of the P or D surfaces (or on the sphere, S^2) contains a single triangular motif, bounded by mirror lines intersecting at $\frac{\pi}{2}, \frac{\pi}{3}, \frac{\pi}{4}$ (Fig. 2a). The relevant orbifold symbol string is thus *234. (Note that cyclic permutation of ordering of rotation center symbols and mirror intersection is allowed.) Following Coxeter, we call orbifolds such as *234 — containing only mirror strings — kaleidoscopic.

Table 1. Character strings (a and b denote integers) and costs associated with 2D symmetry elements of orbifolds. The orbifold characteristic is calculated from these costs (Eq. (1)). The string nomenclature is applicable to any 2D symmetric pattern, whether it is elliptic, planar or hyperbolic. (Crystallographic point groups are elliptic, 2D planar groups are Euclidean.)

Symmetry element	Symbol	cost, c_i
Mirror	*	1
a-fold rotation center	a	$\frac{a-1}{a}$
Mirror intersection (angle $\frac{\pi}{b}$)	b	$\frac{b-1}{2b}$

The symbol string allows direct reckoning of the characteristic of the orbifold, *via* the equation:

$$\chi = 2 - \sum_i c_i \qquad (1)$$

where c_i values are associated with each character entry in the orbifold symbol (Tab. 1). This characteristic coincides with the topological Euler-Poincaré characteristic, and scales linearly with the integral Gaussian curvature of the asymmetric domain in the relevant 2D space. Since the spaces are of constant Gaussian curvature, the Gauss-Bonnet theorem implies that the characteristic also scales with the area of the asymmetric domain. If the characteristic is positive, the geometry is elliptic (point groups); zero implies Euclidean character (plane groups); negative characteristics are associated with hyperbolic space.

A second, concise description of the recipe for determining the relevant kaleidoscopic group of the universal cover of the surface is possible with the orbifold concept. Note first that the Gauss map is defined on the unit sphere, S^2. The reflection symmetries of the Gauss map form a kaleidoscopic elliptic group. Multiplying the order of the mirror points at branch points (i) of the Gauss map by their order, b_i, gives the relevant hyperbolic kaleidoscopic group of the universal cover of the three-periodic minimal surface in H^2. For example, the P, D and H surfaces have exclusively first order branch points, so that the mirror points at flat points must be doubled. The correspondence is illustrated in Table 2.

The conformal map offers a conformally exact — but non-isometric — mapping from H^2 to the three-periodic minimal surfaces. Conformal equivalence means that all angles are preserved between nets drawn on H^2 and the projected nets drawn on the three-periodic surfaces (in E^3). The lack of isometric equivalence means that edge lengths on the nets differ from H^2 to E^3. But the mapping is sufficient to construct nets in E^3 with specified 2D *topology* from those in H^2. Specific sites on H^2 map to sites on the three-periodic surfaces. An explicit transformation from H^2 to C^2 to E^3 can be established, and will be presented elsewhere. For now, we use the vertices and edges of the kaleidoscopic tiling of the surface orbifold as a coordinate net. We call this net the *surface atlas*. The relevant atlases in H^2 for the P, D and H surfaces are shown in Figure 3. We note that hyperbolic n-gons with fixed vertex angles have $(n-3)$ degrees of flexibility in H^2. The metric geometry of the H atlas contains a single free parameter (*e.g.* the ratio of edge lengths in a single *2226 hyperbolic quadrilateral, with vertex angles of $\frac{\pi}{2}$, $\frac{\pi}{2}$, $\frac{\pi}{2}$, $\frac{\pi}{6}$). This one-parameter family corresponds to the family of H surfaces, of variable axial ($\frac{c}{a}$) ratio.

Table 2. Orbifold symmetries for the P, D and H three-periodic minimal surfaces. The surface orbifolds are simple "symmetry mutations" of the orbifold of the Gauss map of the surfaces (Fig. 2).

Surface	Gauss map orbifold (S^2, C^2)	Surface orbifold (H^2)
P, D	*243	*246
H	*3(1)22	*6222

We use a compact, conformal representation of H^2, known as the Poincaré disc model. This model allows the entire hyperbolic plane to be represented in a unit disc in the Euclidean plane, at the expense of much foreshortening of distances while all angles in H^2 are conserved [14]. The correspondence between points on H^2 and points in E^3 (*via* Cartesian coordinates on the three-periodic minimal surfaces) follows at once from the identification of the H^2 orbifold with the C^2 orbifold of the Gauss map, since a constructive map from the C^2 coordinates to E^3 Cartesian coordinates is afforded by the Weierstrass equations defining the minimal surface geometries [10].

The construction leads to three-periodic nets in E^3 with specified 2D ring-size n_2, and edge valency (connectivity) at each vertex, z, whose 2D Schläfli symbol is (n_2, z) in general, and $\{n_2, z\}$ in some cases (with regular n_2-gons). Collar rings are invisible in the universal cover (H^2); they are not prescribed *a priori*. Just as for graphitic tubule nets of distinct chirality (and screw dislocation strength), multiple nets 3D nets can be constructed sharing the same surface rings, but displaying different collar rings. (A lengthy introduction to our approach has been presented elsewhere [15].)

We illustrate the technique with some examples of network topologies that are difficult to realize within the context of 3D Euclidean space. In particular, we construct examples of (3, 7), (5, 4) and (5, 5) reticulations of the P and D surfaces. The first example is of fundamental interest: it is the simplest hyperbolic analog of the regular close-packing pattern of identical discs in E^2 (*i.e.* $\{3, 6\}$) and its seven-fold connectivity cannot be realized as a regular net in E^3. The latter examples, containing pentagonal rings are also of wider interest, due to the geometric frustration of embedding regular pentagonal patterns in E^3.

The crystallography of H^2 is immensely rich compared with 2D (or 3D) Euclidean crystallography. *Any*

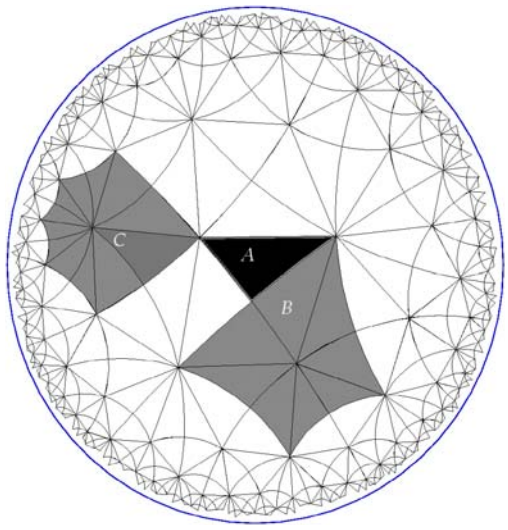

(a)

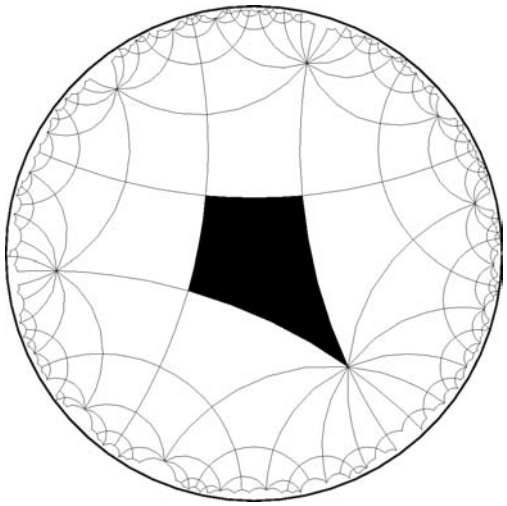

(b)

Fig. 3. Surface atlases of the (a) P, D and (b) H surfaces in the Poincaré disc representation of the hyperbolic plane. The atlas is the universal cover of the surface with the surface orbifold symmetry. Single asymmetric units of (a) the *246 and (b) *6222 orbifolds are shaded black. (a) Single asymmetric tile (A), a single regular tile of the (B) $\{4,6\}$ and (C) dual $\{6,4\}$ tilings on the P and D surface universal covers.

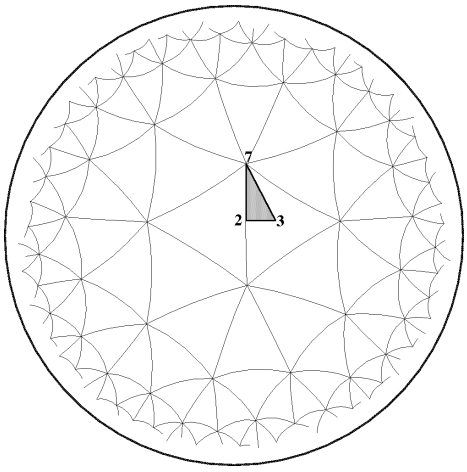

(a)

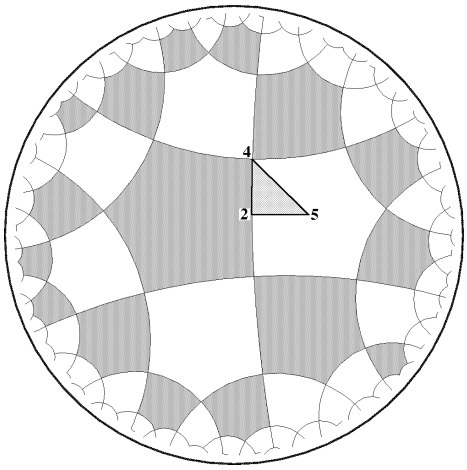

(b)

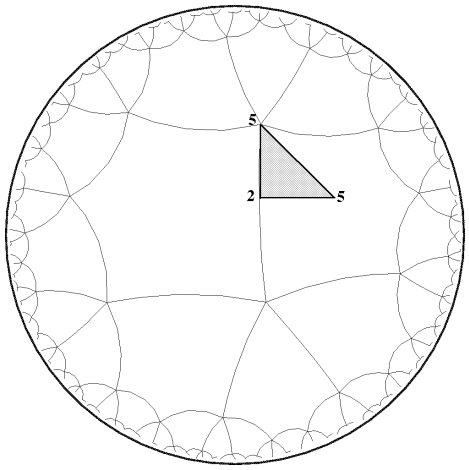

(c)

Fig. 4. Regular hyperbolic tilings with symmetrically identical vertices, edges and faces; (a) $\{3,7\}$ (b) $\{5,4\}$ and (c) $\{5,5\}$. Single triangular domains of the relevant kaleidoscopic orbifolds are outlined by dark edges, lying on mirror lines: (a) the *237, (b) *245 (ignoring the tile colouring) and (c) *255 orbifolds.

net (n_2, z) can be embedded in H^2 such that all vertices, edges and rings are symmetrically equivalent (regular), to form $\{n_2, z\}$. The examples we consider here are shown in Figure 4. These regular nets $\{n_2, z\}$ display pure reflection symmetry: they are decorations of $*n_2z2$ orbifolds.

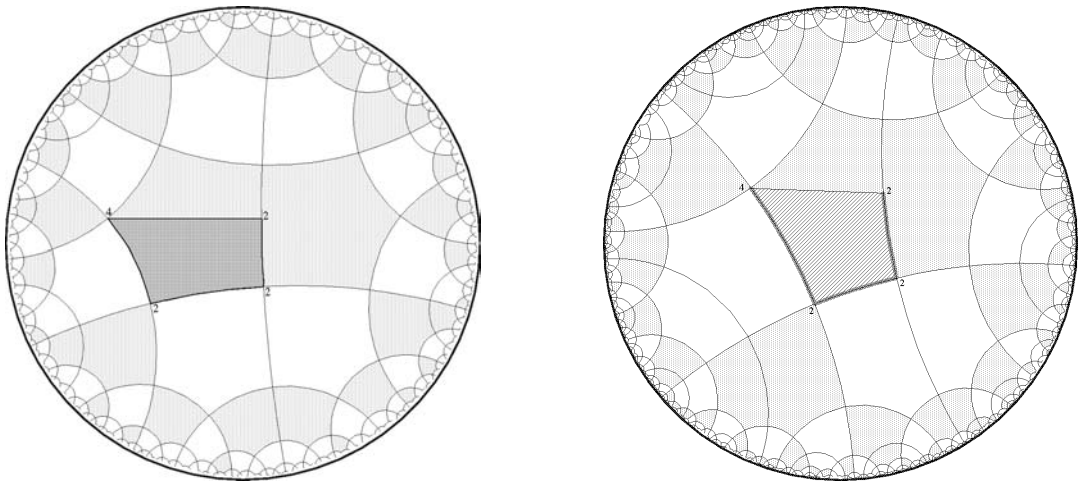

(a) (b)

Fig. 5. (a) Superposition of the regular $\{5,4\}$ tiling on the irregular (6, 4) tiling (with (6) rings shaded alternately grey and white for clarity). A single *2224 quadrilateral orbifold domain is highlighted, bounded by mirrors with vertex angles of $\frac{\pi}{2}$, $\frac{\pi}{2}$, $\frac{\pi}{2}$ and $\frac{\pi}{4}$. (b) Superposition of the regular $\{6,4\}$ tiling (with $\{6\}$ rings shaded alternately grey and white for clarity) on the (5, 4) tiling. A single *2224 orbifold domain is highlighted.

Formation of Euclidean nets

Projections of hyperbolic tilings onto three-periodic surfaces in E^3 generally requires some symmetry reduction of the regular tiling. A sub-group common to both the surface orbifold and the orbifold of the regular tiling must be found. Despite the incommensurability of generic n_2 rings with the structure of E^3 (*e.g.* pentagons and heptagons), symmetric reticulations are possible.

We first construct the (n_2, z) nets in H^2, superposed on the relevant orbifold for the universal cover of the minimal surface. In some cases, that superposition can be done by inspection. The construction can be done more systematically using the following topological constraints. The face- and vertex-densities can be derived using Euler's relation, that relates the Euler characteristic, χ, to the number of vertices, V, edges, E and faces, F, in the network:

$$\chi = V - E + F : \tag{2}$$

$$\chi_F = 1 - \frac{n_2}{2} + \frac{n_2}{z} \tag{3}$$

and

$$\chi_V = 1 - \frac{z}{2} + \frac{z}{n_2} \tag{4}$$

where χ_F and χ_V denote the Euler characteristic per face and vertex respectively. The ratios of those characteristics with the characteristic per surface orbifold determines the number of vertices and faces per surface orbifold.

Consider first the regular $\{4,6\}$ net, or its dual $\{6,4\}$, that comprise a uninodal net in the atlas for the P/D surfaces, and possible superposition of the (5, 4) net on that tiling. A solution is evident by inspection in the Poincaré disc model of H^2; that superposition results in a pattern of symmetry *2224, whose characteristic, from equation (1) is equal to $\frac{-1}{8}$ (Fig. 5). Note that a (6, 4) tiling with *2224 symmetry is, in general, distorted, in contrast to $\{6,4\}$. In common with the *2226 example met above, the geometry of single *2224 domains is not rigid, as the only constraint on their form is the requirement that vertex angles are equal to $\frac{\pi}{2}$, $\frac{\pi}{2}$, $\frac{\pi}{2}$ and $\frac{\pi}{4}$. Domains of the *2224 tiling of H^2 contain a single free parameter, that can be tuned to force the regular $\{5,4\}$ tiling, superposed on an irregular (6, 4) tiling (Fig. 5a) and *vice versa* (Fig. 5b).

As required, *2224 is a sub-group of both the P and D surface orbifold, *246 and the orbifold of the regular $\{5,4\}$ tiling, *245. Is a more symmetric deformation of $\{5,4\}$ allowed? That can be established from the characteristics of these orbifolds, *viz.* $\frac{-1}{24}$ and $\frac{-1}{40}$ respectively. The sub-group index follows at once from the ratios of the relevant orbifold characteristics [13]. Common sub-groups to these orbifolds must have indices that scale according to the ratio of the group characteristics: $\frac{40}{24}$. The most symmetric common sub-groups must therefore be of index 3 in *642 and 5 in *542 with characteristic $\frac{-1}{8}$, equal to that of *2224. We have therefore found a maximally symmetric embedding of (5, 4) in the P and D surfaces.

It is worth pointing out that *2224 is the surface orbifold of the tetragonally distorted family of P and D (minimal) surfaces, the tP and tD surfaces [16]. That can be inferred from the Gauss maps of the tetragonal family [10] (using the algorithm outlined above). It follows at once that a more regular geometric embedding of the (5, 4) net can be realized by projecting onto the tP and tD surfaces. As in the case of the H surface, the single free parameter in the *2224 pattern is manifested in E^3 by the single degree

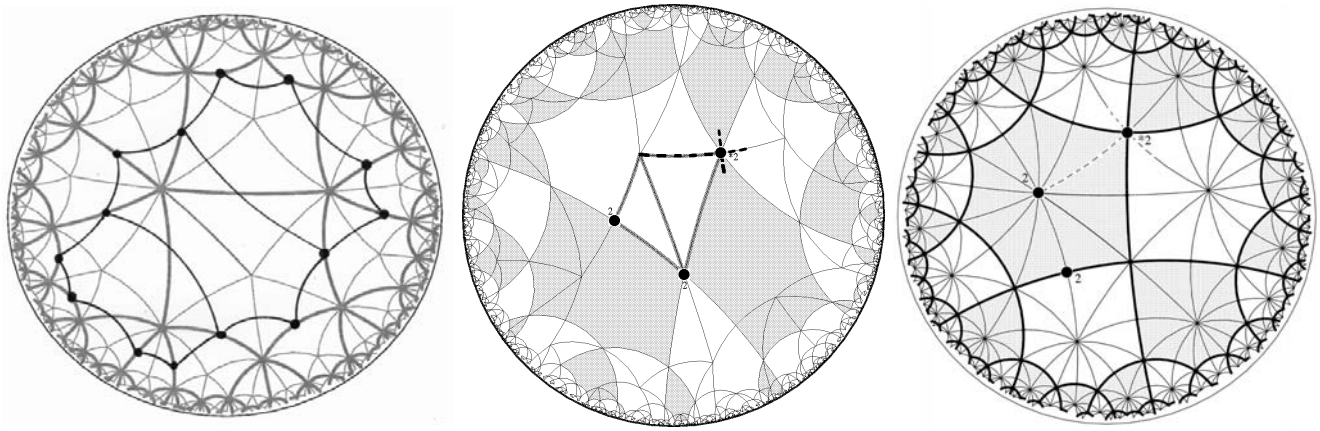

(a) (b) (c)

Fig. 6. (a) Superposition of an irregular (6, 4) net on regular $\{5,5\}$ tiling. The resulting pattern has orbifold symmetry 22*2. Thinner arcs define mirrors of the *255 symmetry of $\{5,5\}$; edges of $\{5,5\}$ are thicker arcs. Vertices of the (6, 4) tiling are marked by dots. (b) A (5,5) net superposed on a $\{6,4\}$ net, with 22*2 symmetry. Edges within a single 22*2 domain are thickened, with "2" entries denoting 2-fold rotational symmetry sites, and the "*2" entry the intersecting of a pair of orthogonal mirrors (dotted lines). (6) tiles are shaded alternately grey and white. (c) The regular $\{6,4\}$ tiling has a subgroup of symmetry 22*2. (b) can therefore be deformed to give (5, 5) on $\{6,4\}$.

of freedom for the tetragonal family of minimal surfaces: the $(\frac{c}{a})$ axial ratio.

Projections of the (5, 4) tilings of symmetry *2224 onto the (cubic) P and D surfaces are shown in Figure 7.

We turn next to the (5, 5) tiling. Here too, the superposition of an irregular (6, 4) tiling on $\{5,5\}$ can be determined by inspection (Fig. 6a). The arrangement of vertices and edges of the $\{5,5\}$ net relative to (6, 4) provides a topological connection diagram to reconstruct an irregular (5, 5) on $\{6,4\}$, allowing projection to the P and D surfaces. We use that map to superpose the (irregular) (5, 5) tiling on the (regular) $\{6,4\}$ tiling (Fig. 6b). The resulting orbifold symmetry is 22*2, with characteristic $\frac{-1}{4}$. This orbifold is a sub-group of index 5 relative to the regular $\{5,5\}$ tiling (*552 orbifold) and index 6 relative to the *642 surface orbifold of the P and D surfaces. Given that the ratio of characteristics of the *552 to *642 orbifolds is $\frac{24}{20}$, the sub-group index ratio of $\frac{6}{5}$ implies, once again, that the pattern is maximally symmetric.

The 22*2 pattern is flexible. Indeed, a specific example of the pattern contains the regular $\{6,4\}$ tiling (Fig. 6c), proving that the superposition of (5, 5) on $\{6,4\}$ is feasible in H^2.

The projections of this net onto the P and D surfaces are shown in Figure 8. Straightened examples, with all edges geodesic in E^3, are also shown. These nets exhibit complex and interesting structures. The projection process forms 4-sided collar rings in both cases. The P version, which adopts a tetragonal symmetry, contains a pair of inclined, slightly distorted, graphite network stacks ((6,3), each with rectangular symmetry), rotated by $\frac{1}{4}/2$ with respect to each other. Inclined layers are linked by connections surrounding a 4_1 screw axis, inducing an overall chirality in the net. That chirality is evident from the orbifold decoration (Fig. 6a): the bilateral symmetry of the orbifold domain has been broken, and there is an arbitrary choice of two possible diagonal edge orientations. Chirality of the net is visible within the hyperbolic plane pattern, an attractive feature of this technique [15].

We close with examples of (3, 7) nets. First, consider in generality the vertex density of (3, 7) on the (4, 6) tiling. From equations (3–4), it is clear that the (3, 7) has two 2 vertices per 4-ring of the (4, 6) tiling respectively. We choose two possible configurations; (i) four (half) vertices, one on each edge of the 4-ring, and (ii) two vertices within the 4-ring. Both can be extended symmetrically; the former with 2323 orbifold symmetry (Figs. 9a, b) and the latter with 2223 orbifold symmetry (Fig. 9d). The 2323 pattern contains two distinct 3-fold and 2-fold sites, most readily seen in the coloured tiling of Figure 9a. In common with the previous examples, both 2323 and 2223 patterns contain significant geometric flexibility. Again, specific examples of both are possible with (3, 7) superposed on the regular $\{6,4\}$ tiling (Figs. 9c, e).

These 2323 and 2223 (3, 7) patterns can be projected onto the P and D surfaces to give rather irregular nets (Figs. 10, 11). The irregularity is particularly evident in the projected (3, 7) patterns with 2223 symmetry, where extreme crowding of adjacent edges is evident on both the P and D projections (Figs. 11a, c). Nevertheless, "relaxation" of the nets by relative vertex motion in E^3, to force a net with equal edge lengths and maximal E^3 symmetry [2] results in a very uniform net with cubic symmetry (space group Fd$\underline{3}$). (Detailed discussion of the relaxation and symmetrisation process in E^3 can be found elsewhere [17].) The edges are those of an array of regular icosahedra, interlinked in a diamond-like geometry by

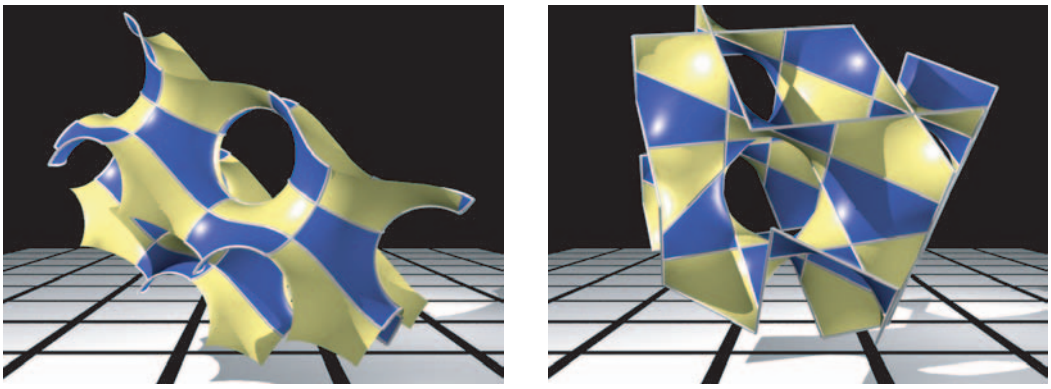

(a) (b)

Fig. 7. Projections of (5, 4) onto the (a) P and (b) D minimal surfaces according to the superposition described in Figure 5b.

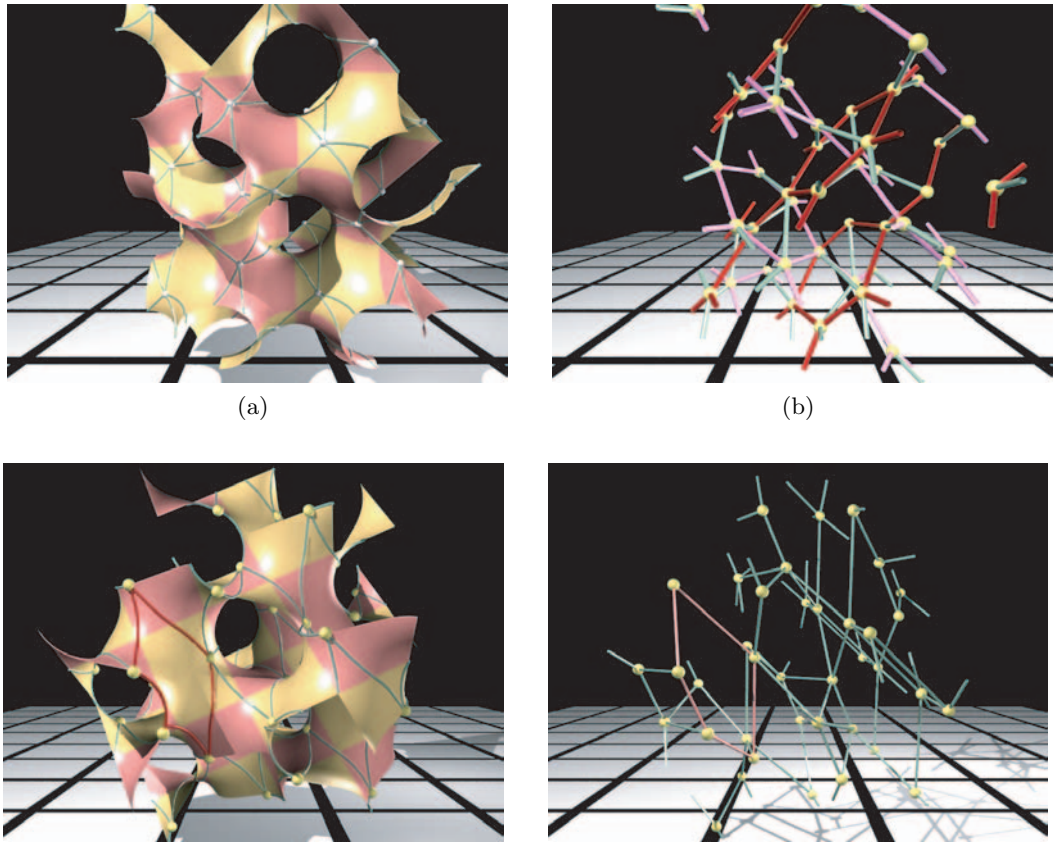

(a) (b)

(c) (d)

Fig. 8. Projections of $\{5,5\}$ nets onto the (a) P and (c) D surfaces. (b) and (d) have identical vertex positions to those in (a) and (c) respectively, with straightened edges. The presence of intergrown irregular (6, 3) graphite-like layers in (b) is highlighted by the edge colouring; parallel stacks of (6, 3) layers are coloured red and magenta, depending on the layer orientation.

face-sharing with regular octahedra [2]. This embedding is conjectured to be the least dense stable sphere packing [2].

The 2223 orbifold has characteristic $\frac{-1}{6}$ (index 4 and 14 relative to the *246 and *237 orbifolds respectively); the 2323 pattern has characteristic $-\frac{1}{3}$ (index 8 and 28 relative to the *246 and *237 orbifolds respectively). The ratio of characteristics of the regular $\{3,7\}$ (*237) and *246 orbifolds is equal to $\frac{84}{24}$, implying the possibility of a maximally symmetric common sub-group of index 2 relative to *246 and 7 relative to *237, with characteristic $\frac{-1}{12}$. Therefore, the possibility of a more symmetric (3, 7) pattern on $\{4,6\}$ cannot be ruled out *a priori*, though we are unable to identify such an example.

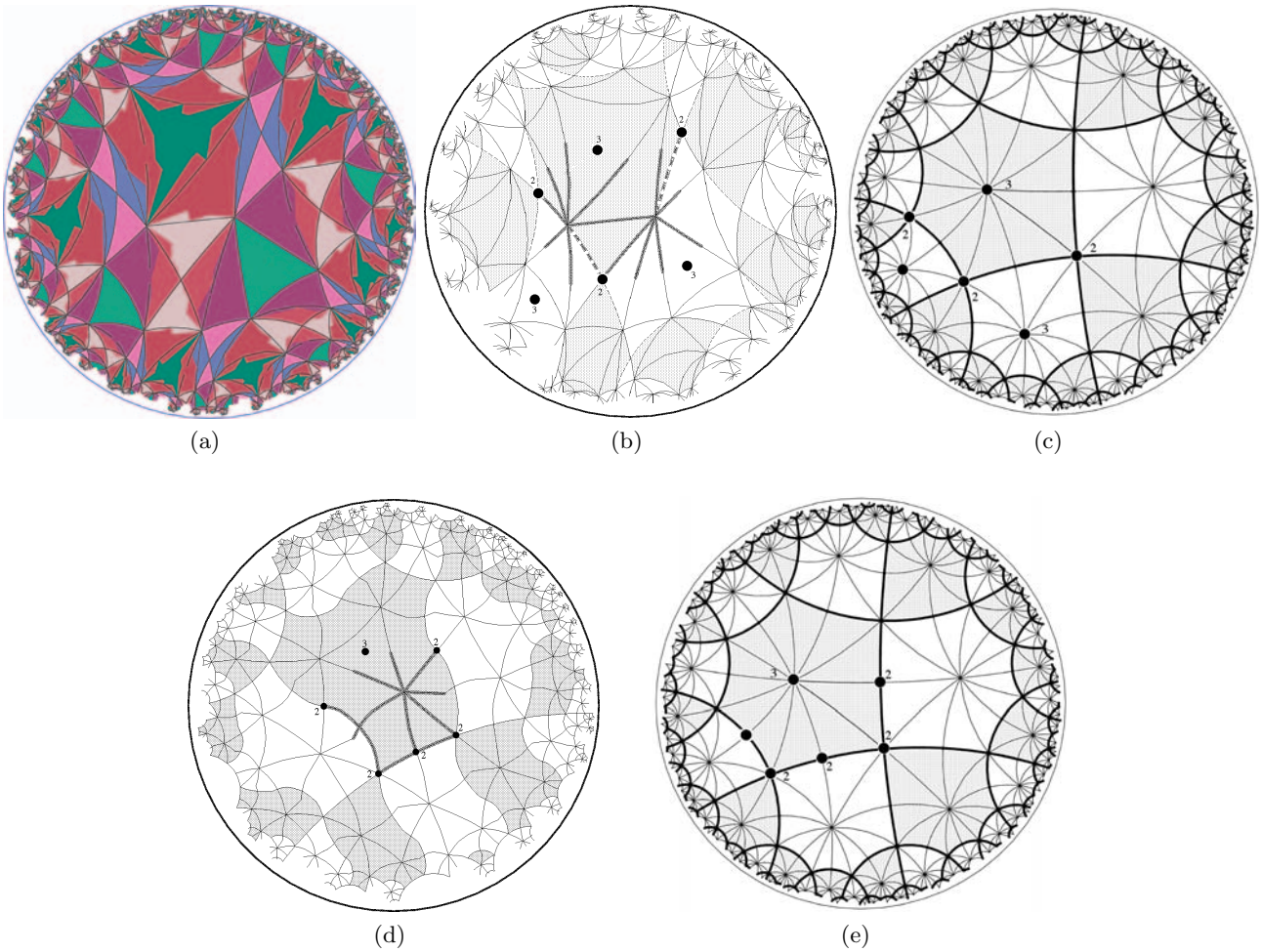

Fig. 9. (a) Superpositions of an irregular (6, 4) net on the (3, 7) tiling. The resulting pattern has orbifold symmetry 2323. The pattern is coloured to mark distinct 2-fold and 3-fold sites. (b) The same tiling, with rotation centers within a single orbifold domain marked by dots (of orders 2 and 3). Thicker arcs belong to a single orbifold of the (3, 7) tiling; dotted arcs are appended to complete the complement of edges of the (6, 4) tiling within a single orbifold. (c) The regular $\{6, 4\}$ tiling has a subgroup of symmetry 2323. (b) can therefore be deformed to give (3, 7) on $\{6, 4\}$. (d) Superposition of (3, 7) on (6, 4) with 2223 symmetry. Thicker arcs belong to a single orbifold of the (3, 7) tiling. Rotation centers within a single orbifold domain are marked by dots. (e) The regular $\{6, 4\}$ tiling has a subgroup of symmetry 2223. (d) can therefore be deformed to give (3, 7) on $\{6, 4\}$. (6) tiles are shaded alternately grey and white in (b–d) for clarity.

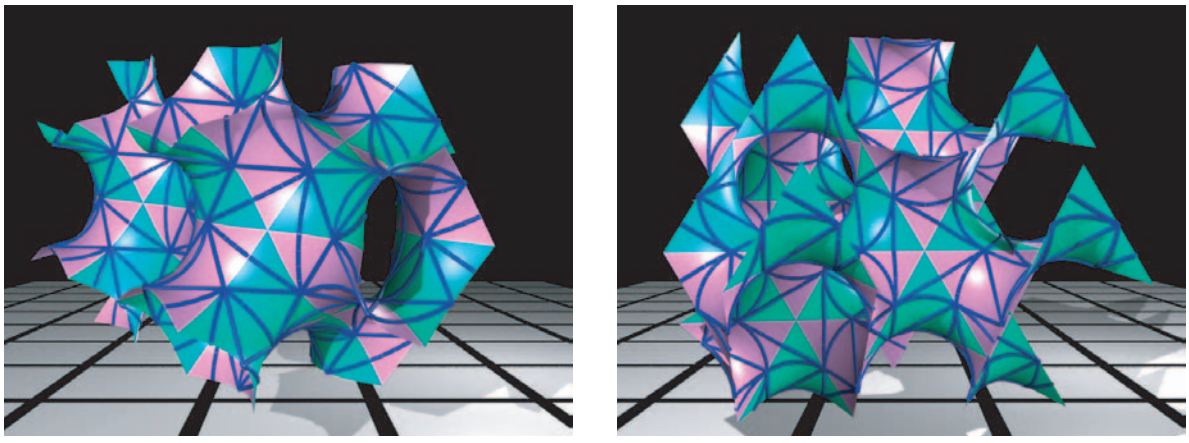

Fig. 10. (a, b) Projections of the 2323 pattern on the P and D surfaces respectively.

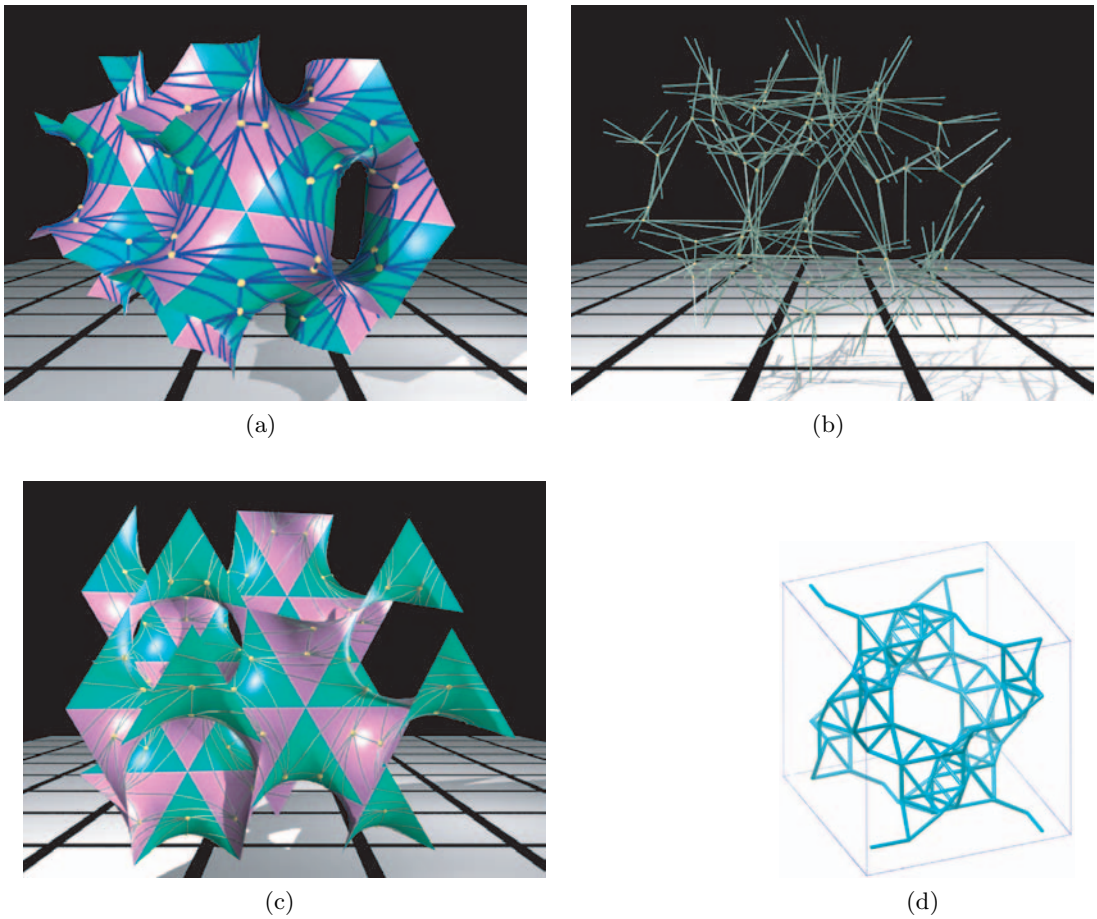

Fig. 11. (a, c) Projections of the 2223 pattern onto the P and D surfaces respectively. (b) Straightened version of (a), with fixed vertices (at identical sites to those in (a)) and straight edges. (d) Single cubic unit cell of a relaxed version of (c), a known very low density stable sphere packing [2].

Outlook

Finally, we mention the possibility of mapping these hyperbolic patterns onto other three-periodic minimal surfaces. The procedure is not limited to the simpler three-periodic minimal surfaces. The atlas for the H surface, illustrated in Figures 2–3, allows construction of reticulations of that surface. Similarly, higher genus surfaces, such as the I-WP surface can be handled. (Indeed, the orbifold defining the surface atlas of the I-WP surface — *2424 — is readily related to that of the P and D surfaces.)

We intend to automatically generate networks in E^3 with the technique outlined in this paper. Given the richness of hyperbolic tilings, we expect some novel structures to emerge. The examples shown here demonstrate that possibility. The major challenge is likely to be the choice of an optimal "basis set" likely to lead to the most regular nets in E^3. We are faced with an embarrassing wealth of possibilities, both in numbers of hyperbolic tilings and variety of surfaces in E^3 to reticulate. The examples presented here are based on the P and D surfaces only. However, the variety of forms realised in those cases alone suggests that we can choose a small set of surfaces to reticulate without compromising the variety of resulting nets.

We thank Daniel Huson for his public domain Funtiles package [18], that was used to draw the Poincaré disc patterns displayed here.

Appendix: Generation of hyperbolic patterns

The H^2 tiling images have been generated using the public domain software Funtiles written by Daniel Huson [18]. The package relies on Delaney-Dress tiling theory, described in detail elsewhere by Huson and colleagues [6,19–21]. Their approach is to encode the tiling pattern and symmetry by decomposition of the (2D) tiling into simplices, whose vertices lie on a face (2-vertex), edge (1-vertex) and vertex (0-vertex) of the original tiling. (The restriction to 2D is ours only: the approach is immediately generalisable to arbitrary dimensions.) Edges of the simplices are labeled by the index of the opposite vertex in that simplex (0,1 or 2). Simplices are labeled according to the symmetry of the pattern; symmetrically identical

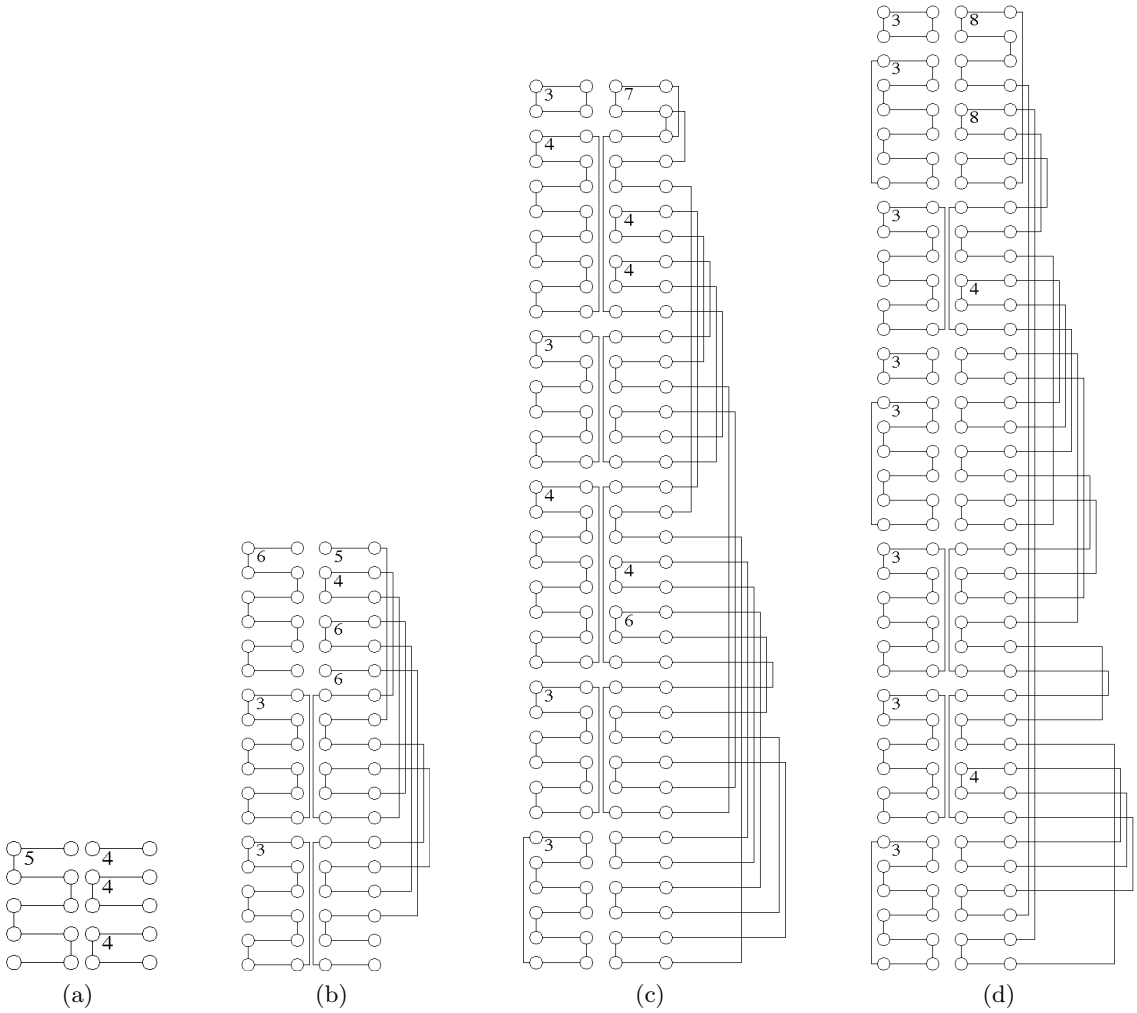

Fig. A.1. Conway crank diagrams for the (a) (5, 4)+(6, 4) tiling (symmetry *2224) shown in Figure 5a, (b) (5, 5)+(6, 4) tiling of Figure 6a (symmetry 22*2), (c) (3, 7)+(6, 4) tiling (symmetry 2223) of Figure 9b and (d) (3, 7)+(6, 4) tiling (symmetry 2323) in Figure 9d.

simplices carry identical labels. (Regular tilings have a single simplex only, the least symmetric (n, z) tilings have at most $2n$ simplices and $2z$ simplices per distinct face and edge respectively.) Involutions between adjacent simplices are characterized by the label of the common simplex edge: *e.g.* a simplex of label A adjacent to one of label B, with common simplex edge 2 implies {A,B} lie within the class of 2-involutions. The resulting encoding allows for an efficient tiling signature. A related concept has been suggested to us by John Conway (private communication); we call the notation *Conway cranks*. Distinct simplices are arranged in columns with one row per simplex. Involutions between distinct simplices by 0, 1 or 2-edges are coded by cranks linking those simplex entries in the 0, 1 or 2 column. The columns contain 0-1 and 1-2 pairs, in order to collect face and vertex configurations of the original tiling respectively. The topology of each face and vertex connectivity is appended by adding the relevant digit to each component of the Conway cranks (face order, n and connectivity, z). The presence of symmetry elements can be discerned by inspection from the crankshaft topology, in common with the symmetry identification from Delaney-Dress symbols [20]. For example, mirror lines lead to (open) chains in the crankshaft diagram, while rotation centres lead to (closed) cycles. Conway cranks for the relevant H^2 tilings, (3,7), (5,4) and (5,5), are shown in Figure A.1. (The apparent reduced complexity of 0-1 and 1-2 cycles (faces and vertices respectively) is induced by the ordering of simplices we have chosen; shuffling of row orders is possible, provided the crankshaft topology is unchanged.) These diagrams afford a concise signature of the tilings, and possible linkages of the Conway cranks consistent with the orders of n and z allow exhaustive listing of allowed tilings [20].

References

1. J.F. Sadoc, R. Mosseri, *Geometrical Frustration* (Cambridge University Press, Cambridge, 1999)
2. M. O'Keeffe, B.G. Hyde, *Crystal Structures 1. Patterns and Symmetry* (Appendix 3) (Mineralogical Society of America, Washington D.C., 1996)
3. Some fascinating additional conjectures can be found in reference [2]
4. M. O'Keeffe, M. Eddaoudi, H. Li, T. Reineke, O.M. Yaghi, J. Sol State Chem. **152**, 3 (2000)
5. D.J. Watts, *Small Worlds* (Princeton University Press, Princeton, 1999)
6. O.D. Friedrichs, A.W.M. Dress, D.H. Huson, J. Klinowski; A.L. Mackay, Nature **400**, 644 (1999)
7. S. Andersson, Angew. Chem. **22**, 69 (1983)
8. A.L. Mackay, Proc. Roy. Soc. Lond. A **442**, 47 (1993)
9. J. Stillwell, *Geometry of Surfaces* (Springer-Verlag, N.Y., 1992)
10. A. Fogden, S.T. Hyde, Acta Cryst. A **48**, 442–451, 575–591 (1992)
11. S.T. Hyde, C. Oguey, Eur. Phys. J. B **16**, 613 (2000)
12. J.-F. Sadoc, J. Charvolin, Acta Cryst. A **45**, 10 (1989)
13. J.H. Conway, in Groups, *Combinatorics and Geometry*, London Mathematical Society Lecture Notes (Cambridge University Press, Cambridge, 1992)
14. D. Hilbert, S. Cohn-Vossen, *Geometry and the Imagination* (Chelsea Publishing Company, N.Y., 1952)
15. S.T. Hyde, S. Ramsden, in *Chemical Topology. Applications and Techniques*, Mathematical Chemistry Series, Vol. 6; edited by D. Bonchev, D.H. Rouvray (Gordon and Breach Science Publishers, Amsterdam, 2000)
16. S. Lidin, J. Phys. France **49**, 421 (1988)
17. S.T. Hyde, S. Ramsden, T. Di Matteo, J. Longdell, Solid State Sci., in press (2003)
18. `www.mathematik.uni-bielefeld.de/huson/papers.html`
19. D.H. Huson, Geometriae Dedicata **47**, 269 (1993)
20. L. Balke, D.H. Huson, Geometriae Dedicata **60**, 89 (1996)
21. O. Delgado Friedrichs, `www.mathematik.uni-bielefeld.de/delgado/TCS/text.html`
22. J.H. Conway (private communication, 1999)